Optical and Quantum Electronics (2022) 54:181
https://doi.org/10.1007/s11082-021-03467-w

Optical modulator using ultra-thin silicon waveguide in SOI hybrid technology

Ahmed B. Ayoub[1] · **Mohamed A. Swillam**[1]

Received: 8 June 2021 / Accepted: 11 December 2021 / Published online: 25 February 2022
© The Author(s), under exclusive licence to Springer Science+Business Media, LLC, part of Springer Nature 2022

Abstract
We propose a detailed study of an on-chip optical modulator using a non-conventional silicon-based platform. This platform is based on the optimum design of ultra-thin silicon on insulator waveguide. This platform is characterized by low field confinement inside the core waveguide and high sensitivity to the cladding index. Accordingly, it lends itself to a wide range of applications, such as sensing and optical modulation. By employing this waveguide into the Mach–Zehnder interferometer configuration, an efficient optical modulator is reported using an organic polymer as an active material for the electro-optic effect. An extinction ratio of more than 20 dB is achieved with energy per bit of 13.21 fJ/bit for 0.5 V applied voltage. This studied platform shows promising and adequate performance for modulation applications. It is cheap and easy to fabricate.

Keywords Interference · Modulation · Photonic structures · Mach–Zehnder interferometer · Ultra-thin

1 Introduction

Silicon Photonics is a CMOS-compatible platform technology that is power-efficient while approaching operating speed comparable to that of light (Reed et al. 2010). Aiming at high-bandwidth systems with high operating speed, electronic and photonic circuits were integrated as in data-communication systems, which resulted in systems with outstanding speed rates and lower power losses. Besides, photonic integrated circuits have been employed in different applications, including optical modulation, and sensing (Reed et al. 2010; Ozbay et al. 2006; Fernandez et al. 2016).

This article is part of the Topical Collection on Optical and Quantum Sciences in Africa.

Guest edited by Salah Obayya, Alex Quandt, Andrew Forbes, Malik Maaza, Abdelmajid Belafhal and Mohamed Farhat.

✉ Mohamed A. Swillam
m.swillam@aucegypt.edu

[1] Department of Physics, School of Sciences and Engineering, The American University in Cairo, AUC Avenue New Cairo, P.O. Box 74, Cairo 11830, Egypt

Optical modulators play a vital role in optoelectronic systems. Thanks to these components, electronic signals are converted to optical signals that propagate using optical waveguides (Reed et al. 2010). Commonly, optical modulation is done either through an Electro-optic effect (i.e., Pockels, Kerr) or a thermo-optic effect (Reed et al. 2010). While silicon lacks electro-optic effects, it has a high thermo-optical property at low speed (i.e., it cannot be employed in high-speed communication systems) (Cocorullo et al. 1992).

Various photonic based modulating structures have been demonstrated (Alloatti et al. 2014; Xiao et al. 2013). A silicon-organic hybrid modulator was proposed (Alloatti et al. 2014) that operates at frequencies up to 100 GHz and beyond so that it can be used in electronic-photonic processing at high speed. Despite its large length of 500 µm, phase efficiency of 11 V.mm, and a capacitance per length of about 100 fF/mm with a parasitic resistance of few Giga-ohms. A high-speed silicon Mach–Zehnder modulator (MZM) with a low insertion loss of 1.9 dB was demonstrated (Xiao et al. 2013). Phase efficiency of less than 2 V·cm was achieved despite an arm length of 750 µm. High-performance modulation with an extinction ratio of 7.5 dB was delivered at 50 Gbps at the expense of an additional optical loss.

An MZM based on Lithium Niobate (LN) of thickness 600 nm on the top of silicon-on-insulator (SOI) photonic circuit was demonstrated in (Weigel et al. 2018). For modulation, aluminum electrodes were placed on the top of the LN layer. Having a long device with 5 mm as the arm length, the authors demonstrated a Phase efficiency of 6.7Vcm and an extinction ratio more than 20 dB. In addition, they demonstrated an ultra-high bandwidth exceeding 106 GHz.

Although LN has been widely used in modulation application, they usually suffer from etching difficulty which usually produces rough surfaces that results in high scattering losses around 3 dB/cm (Wang et al. 2018a; Bahadori et al. 2019). That was until 2017, where M. Zhang, et.al demonstrated LN waveguide with losses as low as ~0.027 dB/cm (Zhang et al. 2017). MZM structure was demonstrated with a LN layer with thickness of 600 nm with arm length of 20 mm (Wang et al. 2018b). In that paper, the authors demonstrated an extinction ratio of 30 dB. Such a modulator allows direct driving by a CMOS circuit while the bandwidth of a similar 5-mm device reaches 100 GHz.

Another approach for optical modulation is based on Electro-optic polymers rather than lithium niobate. Polymers with $r33$ exceeding 300 pm/V are available (Luo et al. 2007; Dalton et al. 2010). Chromophores hyperpolarizability predicts an $r33$ values even above 1000 pm/V. Such $r33$ values are higher than the reported $r33$ values of LN by an order of magnitude or more. On the other hand, the refractive index for such EO polymers are in the range of 1.5–1.7 in the near-infrared range and even at microwave frequencies.

The used of EO polymers has been idely investigated for optical modulation in the recent years (Zhang et al. 2013a; Lin et al. 2010; Wang et al. 2011; Zhang et al. 2013; Zhang et al. 2016). Such devices showed high efficiency in terms of the phase efficiency, the bandwidth, and also the extinction ratio. Further studies reported a photonic crystal based EO modulator that is The 300-µm-long that exhibits a $V\pi$~0.97 V ($V\pi L = 0.29$ Vmm) (Zhang et al. 2013). Slightly improved performance was reported with an improved measured EO BW of 15 GHz (Zhang et al. 2016).

Using silicon-slab waveguides, EO polymer layer was added as a cladding for the waveguide structure (Baehr-Jones et al. 2008; Ding et al. 2010; Hochberg et al. 2007, Sato et al. 2017; Zwickel et al. 2020). Experimental demonstrations reported promising results with phase efficiency below 1Vcm (Baehr-Jones et al. 2008; Ding et al. 2010). More recently, tt was demonstrated in (Sato et al. 2017) that with an ultrathin (50 nm) silicon core with an

overlaying EO polymer layer that a $V\pi$ of 0.9 V was measured together with a 3-dB bandwidth of 23 GHz for a 10-mm-long device.

It appears from the paragraphs above that most of the current silicon photonics-based modulators are based on few hundreds of nanometer waveguide width that requires electron beam lithography technology (EBL) for fabricating these waveguides. Alternatively, it can be fabricated with a high-quality mask with a submicron dimension. However, this mask is also expensive and requires specialized technology to be produced.

Therefore, the need for a new platform for designing photonic structures with standard fabrication technology is necessary. With the proposed platform, standard and straightforward fabrication technology can be employed to fabricate structures with dimensions of more than 1.0 microns. Allowing for standard technology for mask preparation and effectively alleviate the need for EBL technology. On the other hand, the suggested platform also has a unique feature for being more sensitive than other larger waveguide platforms such as ridge configuration, as will be explained through the manuscript.

The paper is organized as follows: Sect. 2 describes the properties of the proposed platform, Sect. 3 studies the photonic modulator based on the proposed platform, and finally, Sect. 4 concludes the paper.

2 Ultra thin waveguide properties

Several studies previously proposed a similar platform to the one proposed in this work (Baehr-Jones et al. 2008; Ding et al. 2010; Hochberg et al. 2007; Sato et al. 2017; Zwickel et al. 2020; Qiu et al. 2015; He et al. 2012; Zou et al. 2015; Abdeen et al. 2016;Ayoub et al. 2017a; Ayoub et al. 2018). The proposed platform is based on an ultra-thin SOI that supports the fundamental mode, as would be seen in a conventional SOI (t = 220 nm, W = 400 nm). The silicon waveguide is shown in Fig. 1, it has a thin thickness (t) of only 50 nm.

The ultra-thin SOI technology supports only the TE mode owing to the small thickness. TE mode is defined by the mode whose major component is along the longer dimension in the plane of incidence (major electric field component along "W"). Due to the small thickness, the TE mode has a low confinement factor inside the waveguide as shown in Fig. 1b (Abdeen et al. 2016; Ayoub et al. 2017a; Ayoub et al. 2018; Ayoub et al., 2017b). The mode profile in Fig. 1b was calculated using the mode solver of Lumerical (Lumerical). On the other hand, TM mode (i.e., major electric field component along "t") can be supported

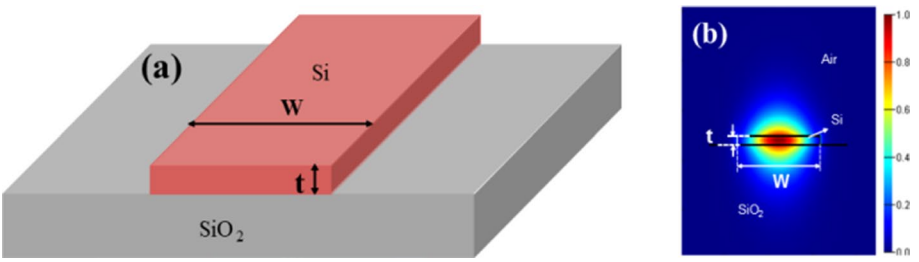

Fig. 1 SOI ultra-thin waveguide structure. **a** Schematic for the physical dimensions of the ultra-thin waveguide. **b** Mode profile for the ultra-thin waveguide

by expanding the thickness (t) of the waveguide as in a conventional waveguide that has a thickness of 220 nm. However, if t = 50 nm, regardless of (W), TM mode will not be supported by the waveguide.

In the SOI geometry, it is assumed that the surrounding is air, while the substrate is silicon dioxide (SiO_2) with a thickness of 1 μm to avoid leakage to the silicon wafer. Substrate leakage loss attenuation is given by the following Eq. (1) (Baehr-Jones et al. 2004):

$$\alpha_{leak} = e^{-2\left(\sqrt{n_{eff}^2 - n_0^2}\right)k_0 A} \tag{1}$$

where $k_0 = \frac{2\pi}{\lambda_0}$ is the free space wavenumber, n_{eff} is the effective index of the mode, n_0 is the effective index of the oxide layer, and A is the thickness of the oxide, in which for the given parameters (λ_0=1550 nm, n_{eff}=1.55, n_0=1.45, A=1 μm),$\alpha_{leak} = 0.011$. Such value can be further suppressed by increasing the thickness (A) to 2–3 μm.

Modal analysis was done by varying the dimensions of the waveguide cross-section using mode solver of Lumerical (Lumerical).

We used Lumerical MODE for mode solving of the waveguide. An override mesh region was added for the ultra-thin silicon waveguide region to save the computational time and power. The mesh size in the override mesh region was set to 5 nm which is 10 times smaller than the dimension we used in our simulations.

The effect of changing the width of the waveguide "W" on the effective refractive index of the structure while keeping t = 50 nm is shown in Fig. 2. Only the first fundamental mode is supported with 700 nm < W < 2 μm, no modes are supported when W < 700 nm. On the other hand, multi-modes are supported given W > 2 μm. Throughout the paper, silicon waveguide with parameters (t = 50 nm, W = 2 μm) will be used. This waveguide can be fabricated using the standard fabrication process for the conventional waveguide. The fabrication steps are performed as follows: (1) performing a partial etching on silicon on insulator platform to get the required thickness (i.e., t = 50 nm), (2) then performing mask lithography, (3) development of the wafer, (4) performing the dry etching process to etch the unneeded Si layer, and (5) finally remove the etchant to reach the final structure. Fabrication tolerance will not affect the overall performance, as seen in Fig. 2 in which the n_{eff} is not oscillating as a function of the width, the fact that compensates the fabrication tolerances due to large width.

Referring to the work in Ref. (Qiu et al. 2015), field penetration into the EO polymer was preserved for thicknesses between t = 10 nm and t = 60 nm with the penetration linearly increases as the thickness decreases. However, the simulation results shows that the optical losses dramatically increases as the waveguide thickness decreases and therefore

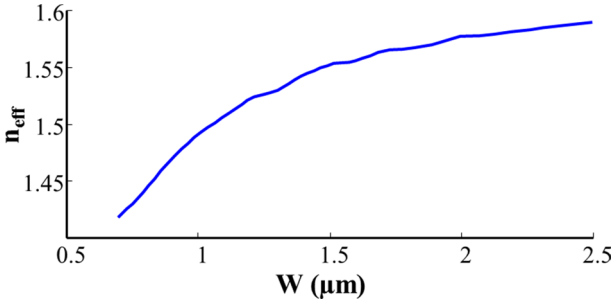

Fig. 2 The effect of changing the waveguide width on the effective index. The substrate is assumed to be SiO_2 with air as the surrounding

t = 30 nm was selected as the optimum thickness in their design. Referring to the fabrication tolerances, as shown in Ref (Qiu et al. 2015), they showed that using inductively coupled plasma (ICP) etching with SF6 gas, they could reach the desired thickness of t = 30 nm which is already less than the thickness we aim at in our design. In addition in Ref. (Zou et al. 2015), they showed that using another fabrication technique as explained in (Zhou et al. 2012), they were able to reach a thickness of t = 60 nm.

During the computational analysis, the MZI has an arm length of 350 μm and a bending radius of 80 μm. The propagation loss is calculated for the waveguide to know the limitations on the arm length. A propagation loss of 0.024 dB/cm is considered an acceptable value for the design of long-arm modulators as compared to loss values reported in (Qiu et al. 2015). However, additional terms can include the bending loss of the MZI, which is in the range of 2.5 dB/cm at a bending radius of 80 μm. Adding a surface roughness of 3 dB/cm can result in a total loss of around 0.2 dB for an arm length of 350 μm. In the following section, an ultra-thin MZI optical modulator is discussed in detail. A comparison with other modulation systems is also performed.

3 Ultra thin waveguide based photonic modulator

3.1 MZI based photonic modulator

Electromagnetic simulations are performed using the commercial Beam Propagation Method (BPM) (Opi-FDTD, Opti-wave]. Assuming polymer with the Pockels electro-optic effect, refractive index change is governed by Eq. (2) (Dalton et al. 1995):

$$\Delta n = \frac{1}{2} n_0^3 r_{33} \frac{V_a}{t_p} \tag{2}$$

where n_o is the polymer refractive index at zero applied voltage and has a value of 1.6, V_a is the applied voltage, t_p is the thickness of the polymer, r_{33} represent the electro-optic effect and has a value of 310 pm/V. This polymer can be retrieved by a 1:1 mixture between (C28H21F3N4OS, molecular weight 518.6) and (C32H28F3N4O, molecular weight 541.6) (Kim et al. 2007). Having $t_p = 200nm$, resulted in a calculated metal absorption loss of 24 dB/cm, yielding a total metal absorption loss of 0.84 dB for an arm length of 350 μm. "On" state is reached when applying voltage $V_a = 2$ V through the metal electrodes resulting in a refractive index change of $\Delta n = 6.35 * 10^{-3}$, as given by Eq. (2).

"On" state is reached when applying voltage V_a through the metal electrodes (silver). Although gold has better resistivity against oxidization than silver, however, it suffers much more than silver in terms of the optical losses which will affect the performance in terms of the output power level. Hence, silver was picked based on this point. In addition, silver is much cheaper for the fabrication process. Applying an applied voltage "V_a" results in changing the refractive index of the polymer by which results in phase shift experienced by the optical mode and hence a phase shifted transmission versus the wavelength. Owing to the geometrical shape of the ultra thin waveguide, the field experience a low confinement in the core waveguide improving the field interaction with the surroundings as shown in Fig. 3b and hence higher extinction ratio can be achieved with much lower arm lengths which will result in a small-size, and lower power consumption optical modulator, making it a promising solution for many modulation applications in low-power photonic systems.

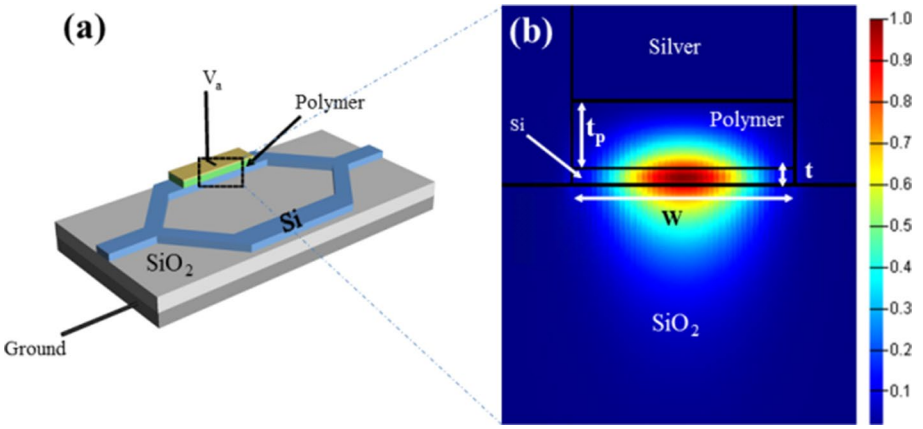

Fig. 3 MZI photonic modulator. **a** Schematic for the ultra-thin waveguide based MZI modulator. **b** mode profile inside the polymer, it shows the strong interaction between the optical mode and the polymer

The refractive index change of the polymer due to an applied voltage is calculated and then the effective index of the cross sectional area of the waveguide is calculated using computational tools. After that the effective index is used inside the BPM commercial tool to calculate the transmission at selected wavelengths.

The schematic of the optical modulator design is shown in Fig. 3a. As discussed in the previous section, the TE mode is weakly confined in the ultra-thin waveguide, allowing for better penetration into the polymer, as shown in Fig. 3b. Field distribution is calculated using the mode solver of Lumerical (Lumerical). High field penetration into the polymer allows for a higher extinction ratio at significantly shorter arm length as compared to conventional SOI systems.

3.2 Modulator results

As mentioned in the previous section, during the computational analysis, the arm length was designed to be 350 μm with a bending radius of 80 μm, with a polymer thickness "t_pε of 200 nm yielding an acceptable capacitance (C) value of 79.27 Ff without dramatically suppressing the performance (Ayoub et al. 2018). Assuming bit-rate (R_{bit}) of 0.1Tbit/sec, the power consumption for a return to zero (RTZ) can be calculated using Eq. (3) (Timurdogan et al. 2014):

$$P = \frac{1}{2} R_{bit} C V_a^2 \tag{3}$$

Assuming applied voltage V_a=2 V, $P = 0.0158$W. Hence, ($E_{bit} = \frac{1}{2} C V_a^2$) equals 158 fJ/bit (Ayoub et al. 2018). The half-wave voltage V_π is calculated using Eq. (4):

$$V_\pi = \frac{\lambda_0 t_p}{n_0^3 r_{33} \zeta} \tag{4}$$

where ζ is the arm length, Given the above parameters, $V_\pi = 0.697$V and $V_\pi \zeta = 2.44 * 10 - 2$V.cm. At an $\lambda_0 = 1550nm$, the extinction ratio (ER) equals 11.3 dB

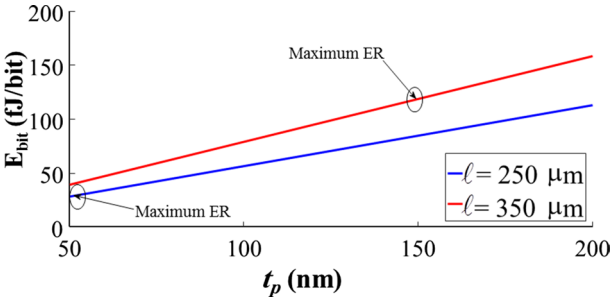

Fig. 4 E_{bit} versus polymer thickness (t_p) for different MZI arm length

Table 1 Relation between the polymer thickness and the modulator key performance parameters at the telecommunication wavelength; 1310 nm and 1550 nm. The arm length here is assumed to be 350 μm with applied voltage 0.5 V. Here the is varying

Polymer thickness (d)	E_{bit} (fJ/bit)	ER (dB)—λ_0 = 1550 nm	ER (dB)—λ_0 = 1310 nm	$V_\Pi.L$(V.m)—λ_0 = 1550 nm	$V_\Pi.L$(V.m)—λ_0 = 1310 nm	Waveguide Losses (dB/mm)
200	9.91	4.43	24.44	$2.44*10^{-4}$	$2.06*10^{-4}$	24
150	13.21	20.36	3.47	$1.83*10^{-4}$	$1.55*10^{-4}$	25
100	19.82	14.06	15.99	$1.22*10^{-4}$	$1.03*10^{-4}$	26
50	39.64	9.63	3.58	$0.61*10^{-4}$	$0.52*10^{-4}$	27

which is given by $\boldsymbol{ER} = 10\boldsymbol{log}\frac{\boldsymbol{P_{on}}}{\boldsymbol{P_{off}}}$; where $\boldsymbol{P_{on}}$,$\boldsymbol{P_{off}}$ is the power in the "On" and "Off" state, respectively (Reed et al. 2010).

Figure 4 shows the effect of changing the polymer thickness on the performance while setting the field $\frac{V_a}{t_p}$ to a certain constant (i.e., Δn has a constant value). A constant field is conserved by varying the $\boldsymbol{V_a}$ for different $\boldsymbol{t_p}$. By doing this analysis, a compromise between ER and E_{bit} is achieved.

In addition, Fig. 4 shows the E_{bit} as a function of the $\boldsymbol{t_p}$ for constant Δn of $6.35*10^{-3}$ at different $\boldsymbol{\zeta}$. The arrows show the positions of the maximum extinction ratio (ER) for each $\boldsymbol{\zeta}$. For a $\boldsymbol{\zeta}$ of 250 μm, a maximum ER of 25.14 dB occurs for $\boldsymbol{t_p}$ of 50 nm while for a $\boldsymbol{\zeta}$ of 350 μm, a maximum ER of 23.02 occurs for $\boldsymbol{t_p}$ of 150 nm. The previous study shows that for maintaining a maximum ER, $\boldsymbol{t_p}$ has to be increased with increasing $\boldsymbol{\zeta}$. On the other side, by changing $\boldsymbol{t_p}$ and $\boldsymbol{\zeta}$, $\boldsymbol{V_\pi}$ will change in which $\boldsymbol{V_\pi}$ is 0.25 V at ($\boldsymbol{\zeta}$ =250 μm, $\boldsymbol{t_p}$= 50 nm) while it is 0.52 V at ($\boldsymbol{\zeta}$ =350 μm, $\boldsymbol{t_p}$= 150 nm) which reflects the trade-off between E_{bit}, and ER, and $\boldsymbol{V_\pi}$ and the need to have an optimized design to compromise between these performance metrics.

Table 1 shows how the energy per bit and the extinction ratio (ER) are affected by the change in the polymer thickness which shows the tradeoff between the energy per bit and the ER.

Table 2 shows the effect of applying different voltages and using different channel lengths on the performance of the modulator in terms of the E_{bit}, ER, and $\boldsymbol{V_\pi\zeta}$ metrics at $\lambda_0 = 1550\boldsymbol{nm}$. As shown in the table, modulator performance varies based on the design parameters selected for the optical design. From Table 2, it could be demonstrated that a polymer having a thickness of 150 nm at an applied voltage of 0.5 V represents

Table 2 Different modulators design performance in terms of E_{bit}, ER, and $V_\pi\zeta$ at $\lambda_0 = 1550nm$

Applied voltage (V)	Polymer thickness t_p (nm)	Energy per bit (E_{bit}) (fJ/bit)	(ER) (dB)	Channel length (ζ) (μm)	$V_\pi\zeta$(V.cm)
2 V	150	151.2	16.8	250	$1.83*10^{-2}$
	150	211.7	20.1	350	$1.83*10^{-2}$
1.5 V	150	84.96	12.97	250	$1.83*10^{-2}$
	150	118.94	23.02	350	$1.83*10^{-2}$
1 V	150	37.76	6.27	250	$1.83*10^{-2}$
	150	52.86	22.44	350	$1.83*10^{-2}$
0.5 V	150	9.44	2.93	250	$1.83*10^{-2}$
	150	13.21	20.36	350	$1.83*10^{-2}$

the best compromise between ER and E_{bit}, and ζ at a wavelength of 1550 nm with an ER = 20.36 dB, E_{bit} = 13.21 fJ/bit, and ζ = 350 μm.

A similar design was demonstrated in (Sato et al. 2017) in which an MZI based modulator with ultra-thin silicon waveguide was fabricated. Although the design looks identical to the proposed design here, the performance of both models is quite different. In (Sato et al. 2017), the MZI-based modulator has a propagation loss of 4 dB/cm compared to 0.024 dB/cm in our paper. Owing to the high electro-optic coefficient of the polymer used here, we believe the ER will surpass the achievable ER in (Sato et al. 2017) (i.e., r_{33} = 310 pm/v in the proposed work, r_{33} = 70 pm/v in (Sato et al. 2017). Besides, we reach E_{bit} as low as 13.21 fJ/bit compared to 30.18 fJ/bit. Table 3 shows the performance of the proposed MZI based modulator as compared to silicon-based modulators previously proposed with different structures. As shown, the proposed model is considered a good compromise between each of ER and E_{bit}. Assuming low doping concentration, the resistivity of silicon is around 10 Ohm.m. Whereas the waveguide has a thickness of 50 nm, and the area equals 350 μm × 2 μm. The resistance is calculated to be 714 ohms. Hence, the speed of the modulator can be estimated to be 17.66 GHz. The maximum modulation bandwidth (f) that can be achieved is inversely proportional to the change in the refractive index and is given by Eq. (5) (Liu et al. 2015):

Table 3 Comparison between the proposed structure and the previously proposed silicon-based modulators

Modulation principle	Modulator structure	ER (dB)	E_{bit} (fJ/bit)
Electro-optic (wang et al. 2018)	MZI	30	–
Electro-optic (sato et al. 2017)	MZI	–	30.18 @V_a = 2 V
Carrier-injection (chen et al. 2009)	Ring	7	120
Carrier-depletion (Dong et al. 2009)	Ring	6.5	50
Electro-optic (Kieninger et al. 2020)	MZI	30	–
Electro-refractive (proposed)	MZI	20.36	13.21

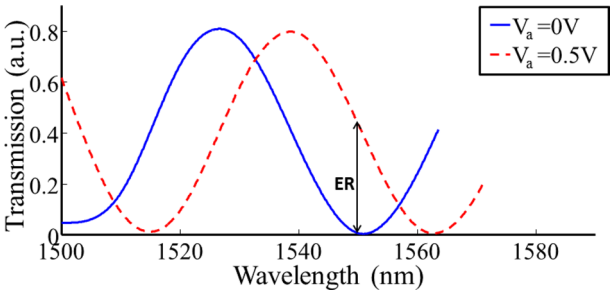

Fig. 5 Transmission versus wavelength in the "On" and "Off" states

$$(f * \zeta)_{max} = \frac{c}{4\Delta n} \tag{5}$$

where c is the speed of light in air. From this equation, for $\Delta n = 6.35 * 10^{-3}$, and arm length ($\zeta$) of 350 µm, $f_{max} = 3.37 * 10^{13}$Hz.

The transmitted intensity is plotted in Fig. 5 as a function of wavelength in which high ER is achieved at 1550 nm with $E_{bit} = 13.21$ fJ/bit (Ayoub and Swillam 2018; 2017b).

4 Conclusion

MZI optical modulator based on the ultra-thin is presented in this paper. An MZI –based modulator is proposed. An extinction ratio of 20.36 dB at 1550 nm with an arm length of 350 µm is reported. With an applied voltage of 0.5 V, the low power consumption of 0.0158 W is achieved at high speed rates.

Acknowledgements This work was made possible by a NPRP award [NPRP 7-456-1-085] from the Qatar National Research Fund (member of the Qatar Foundation). The statements made herein are solely the responsibility of the authors.

Author Contributions ABA conceived the basic idea and validated the concept of operation through computer-aided simulations. MAS supervised the entire project. All the authors contributed to the general discussion and revision of the manuscript.

Data and material availability Authors will make readily reproducible materials described in the manuscript, including new software, databases and all relevant raw data, freely available to any scientist wishing to use them, without breaching participant confidentiality. Authors will make their new software, databases, application/tool described in the manuscript available for testing by reviewers in a way that preserves the reviewers' anonymity.

Declarations

Conflict of interest The authors declare that they have no conflict of interest.

References

Abdeen, A. S., et al.: High efficiency compact Bragg sensor. 2016 Photonics North (PN). (2016)
Alloatti, L., et al.: 100 GHz silicon–organic hybrid modulator. Light Sci. Appl. **3**(5), e173–e173 (2014)
Ayoub, A., Swillam, M.: Ultra-sensitive silicon-photonic on-chip sensor using microfabrication technology, SPIE. (2017)

Ayoub, A. B., Swillam, M. A.: High performance silicon Mach-Zehnder interferometer based photonic modulator. 2017 International Applied Computational Electromagnetics Society Symposium—Italy (ACES). (2017)
Ayoub, A., Swillam, M.: High-performance optical modulator using ultra-thin silicon waveguide in SOI technology, SPIE. (2018)
Baehr-Jones, T., et al.: High-Q ring resonators in thin silicon-on-insulator. Appl. Phys. Lett. **85**(16), 3346–3347 (2004)
Baehr-Jones, T., et al.: Nonlinear polymer-clad silicon slot waveguide modulator with a half wave voltage of 0.25V. Appl. Phys. Lett. **92**, 10, 1663303, 1–3 (2008)
Bahadori, M., et al.: High performance fully etched isotropic microring resonators in thin-film lithium niobate on insulator platform. Opt. Express **27**, 22025–22039 (2019)
Chen, L., et al.: Integrated GHz silicon photonic interconnect with micrometer-scale modulators and detectors. Opt. Express **17**(17), 15248–15256 (2009)
Cocorullo, G., Rendina, I.: Thermo-optical modulation at 1.5μm in silicon etalon. Electron. Lett. **28**, 83–85 (1992)
Dalton, L.R., et al.: Polymeric electro-optic modulators: matereials synthesis and processing. Adv. Mater. **7**(6), 519–540 (1995)
Dalton, L.R., et al.: Electric field poled organic electro-optic materials: state of the art and future prospects. Chem. Rev. **110**, 25–55 (2010)
Ding, R., et al.: Demonstration of a low VπL modulator with GHz bandwidth based on electro-optic polymer-clad silicon slot waveguides. Opt. Express **18**, 15618–15623 (2010)
Dong, P., et al.: Low Vpp, ultralow-energy, compact, high-speed silicon electro-optic modulator. Opt. Express **17**(25), 22484–22490 (2009)
FDE tool: https://www.lumerical.com/
Fernández Gavela, A., et al.: Last advances in silicon-based optical biosensors. Sensors **16**(3), 1–15 (2016)
He, L., et al.: Ultrathin silicon-on-insulator grating couplers. IEEE Photonics Technol. Lett. **24**(24), 2247–2249 (2012)
Hochberg, M., et al.: Towards a millivolt optical modulator with nano-slot waveguides. Opt. Express **15**, 8401–8410 (2007)
Kieninger, C., et al.: Silicon-organic hybrid (SOH) Mach-Zehnder modulators for 100 GBd PAM4 signaling with sub-1 dB phase-shifter loss. Opt. Express **28**, 24693–24707 (2020)
Kim, T.-D., et al.: Ultralarge and thermally stable electro-optic activities from supramolecular self-assembled molecular glasses. J. Am. Chem. Soc. **129**(3), 488–489 (2007)
Lin, C.Y., et al.: Electro-optic polymer infiltrated silicon photonic crystal slot waveguide modulator with 23 dB slow light enhancement. Appl. Phys. Lett. **97**, 093304, 1–4 (2010)
Liu, J., et al.: Recent advances in polymer electro-optic modulators. RSC Adv. **5**, 15784–15794 (2015)
Luo, J., et al.: Phenyltetraene-based nonlinear optical chromophores with enhanced chemical stability and electrooptic activity. Org. Lett. **9**, 4471–4474 (2007)
Opti-FDTD, Opti-wave, Inc. ⟨http://www.optiwave.com⟩
Ozbay, E.: Plasmonics: merging photonics and electronics at nanoscale dimensions. Science **311**(5758), 189–193 (2006)
Qiu, F., et al.: Ultra-thin silicon/electro-optic polymer hybrid waveguide modulators. Appl. Phys. Lett. **107**(12), 123302, 1–6 (2015)
Reed, G.T., et al.: Silicon optical modulators. Nat. Photon. **4**(8), 518–526 (2010)
Sato, H., et al.: Low driving voltage Mach-Zehnder interference modulator constructed from an electro-optic polymer on ultra-thin silicon with a broadband operation. Opt. Express **25**, 768–775 (2017)
Timurdogan, E., et al.: An ultralow power athermal silicon modulator. Nat. Commun. **5**(1), 4008, 1–11 (2014)
Wang, X., et al.: Effective in-device $r33$ of 735 pm/V on electro-optic polymer infiltrated silicon photonic crystal slot waveguides. Opt. Lett. **36**, 882–884 (2011)
Wang, C., et al.: Integrated lithium niobate electro-optic modulators operating at CMOS-compatible voltages. Nature **562**, 101–104 (2018)
Wang, C., et al.: Nanophotonic lithium niobate electro-optic modulators. Opt. Express **26**, 1547–1555 (2018)
Weigel, P.O., et al.: Bonded thin film lithium niobate modulator on a silicon photonics platform exceeding 100 GHz 3-dB electrical modulation bandwidth. Opt. Express **26**, 23728–23739 (2018)
Xiao, X., et al.: High-speed, low-loss silicon Mach-Zehnder modulators with doping optimization. Opt. Express **21**(4), 4116–4125 (2013)

Zhang, X., et al.: Polymer-based hybrid-integrated photonic devices for silicon on-chip modulation and board-level optical interconnects. IEEE J. Sel. Top. Quantum Electron. **19**, 196–210 (2013a)
Zhang, X., et al.: Wide optical spectrum range, subvolt, compact modulator based on an electro-optic polymer refilled silicon slot photonic crystal waveguide. Opt. Lett. **38**, 4931–4934 (2013b)
Zhang, X., et al.: High performance optical modulator based on electro-optic polymer filled silicon slot photonic crystal waveguide. J. Lightwave Technol. **34**, 2941–2951 (2016)
Zhang, M., et al.: Monolithic ultra-high-Q lithium niobate microring resonator. Optica **4**, 1536–1537 (2017)
Zhou, L., Xie, J., Lu, L., Zou, Z., Sun, X., Chen, J.: Coupled-resonator-induced-transparency in cascaded self-coupled optical waveguide (SCOW) resonators. In: Asia Communications and Photonics Conference, OSA Technical Digest (online) (Optical Society of America, 2012), paper ATh4B.2
Zou, Z., et al.: 60-nm-thick basic photonic components and bragg gratings on the silicon-on-insulator platform. Opt. Express **23**(16), 20784–20795 (2015)
Zwickel, H., et al.: Verified equivalent-circuit model for slot-waveguide modulators. Opt. Express **28**, 12951–12976 (2020)

Publisher's Note Springer Nature remains neutral with regard to jurisdictional claims in published maps and institutional affiliations.